



저작자표시-비영리-변경금지 2.0 대한민국

이용자는 아래의 조건을 따르는 경우에 한하여 자유롭게

- 이 저작물을 복제, 배포, 전송, 전시, 공연 및 방송할 수 있습니다.

다음과 같은 조건을 따라야 합니다:



저작자표시. 귀하는 원저작자를 표시하여야 합니다.



비영리. 귀하는 이 저작물을 영리 목적으로 이용할 수 없습니다.



변경금지. 귀하는 이 저작물을 개작, 변형 또는 가공할 수 없습니다.

- 귀하는, 이 저작물의 재이용이나 배포의 경우, 이 저작물에 적용된 이용허락조건을 명확하게 나타내어야 합니다.
- 저작권자로부터 별도의 허가를 받으면 이러한 조건들은 적용되지 않습니다.

저작권법에 따른 이용자의 권리는 위의 내용에 의하여 영향을 받지 않습니다.

이것은 [이용허락규약\(Legal Code\)](#)을 이해하기 쉽게 요약한 것입니다.

[Disclaimer](#)

공학석사학위논문

암 표적형 형광전구체를 담지하고 있는

생체친화성 나노전달체의 제조

Preparation of biocompatible nanocarriers
encapsulating fluorescent precursors for
cancer targeting

2018년 2월

서울대학교 대학원

융합과학부 나노융합전공

정 윤

암 표적형 형광전구체를 담지하고 있는
생체친화성 나노전달체의 제조

Preparation of biocompatible nanocarriers
encapsulating fluorescent precursors for cancer
targeting

지도교수 이 강 원

이 논문을 공학석사 학위논문으로 제출함

2017 년 12 월




서울대학교 대학원

융합과학부 나노융합전공

정 윤

정 윤 의 석사학위논문을 인준함

2017 년 12 월

위 원 장 김연상  (인)
부 위 원 장 이강원  (인)
위 원 송윤규  (인)

Abstract

Preparation of biocompatible nanocarriers encapsulating fluorescent precursors for cancer targeting

Yoon Jeong

Program in Nano Science and Technology

Department of Transdisciplinary Studies

The Graduate School of

Seoul National University

Nanomedicine based on nanotechnology facilitates the development of both therapeutic and diagnostic agents. Especially, fluorescence-based imaging guidance for tumor resection has recently emerged as a fascinating tool using exogenous fluorescent contrast agents with objective and precise information of tumor tissues. However, the most contrast agents cannot inherently offer real-time visual information concerning selectivity and localization of the tumor because of a lack of cancer targeting property and insufficient sensitivity for acquiring fluorescent signal in real-time. For selective and active tumor targeting, these contrast agents were chemically conjugated with targeting moieties such as

antibodies and peptides, which often fail in Food and Drug Administration (FDA) approval due to safety issues. Motivated by this point, we have developed nanocarriers to escape the most issues in regard to the clinical safety. In this study, we have demonstrated selective targeting of cancer cells (including in vivo xenograft models) and targeted “turn-on” fluorescence upon delivery of nanocarriers to achieve excellent sensitivity with high signal-to-noise ratio. Owing to the non-toxic and distinct fluorescence, we expect that our nanocarriers developed in this study will be ‘extremely fast’ to be exploited for clinical use.

Keyword: Cancer, Nanocarrier, Fluorescence, Hyaluronic acid, 5-Aminolevulinic acid, Protoporphyrin IX

Student Number: 2016-26027

Table of Contents

Abstract	3
Table of Contents	5
List of Figures	7
Chapter 1. Introduction	10
Chapter 2. Experimental Methods	12
2.1 Materials	
2.2 Preparation of nanocarriers encapsulating 5-ALA	
2.3 Physicochemical Characterization and Stability Monitoring	
2.4 Determination of Entrapment ratio of 5-ALA	
2.5 Degradation Test by hyaluronidase (HAase)	
2.6 Cell culture	
2.7 Fluorescent imaging of Cellular uptake and Receptor blocking assay	
2.8 Flow cytometry analysis	
2.9 The quantification of PpIX fluorescence induced by 5-ALA NCs	
2.10 Cytotoxicity	
2.11 Cancer-selective targeting in co-culture models	
2.12 Fluorescent Live-cell Imaging	
2.13 Animal studies	
2.14 Immunofluorescence assay	

2.15 Survival rate and Weight variation

Chapter 3. Results and Discussion	23
Chapter 4. Conclusion	31
References	32
Figures	37
Publication List	57
초록 (국문)	58

List of Figures

Main Figures

Figure 1. Schematic illustration of the lighthouse, illuminating cancer cells and selective turn on navigation, and nanocarrier (NC) physicochemical characterization.

Figure 2. *In vitro* cellular uptake analysis to verify selective navigation of fluorescence turn on signals.

Figure 3. *In vitro* selective navigation in a co-culture model

Figure 4. *In vivo* nanocarriers' selective navigation of turn on signals via local delivery.

Supplementary Figures

Supplementary Figure 1. (a). scheme of fabrication steps for homogenous nanocarriers, Water-in-Oil emulsification and phase-transfer from oily phase to water phase. (b) Transmission electron microscopy image of Nanocarrier 1 (NC1) at lower magnification. (c) Dynamic light histogram of NCs stored in deionized water, pH 7.4 at room temperature.

Supplementary Figure 2. The calibration curve fit of 5-ALA using 2,4,6-Trinitrobenzenesulfonic acid (TNBS) kit

Supplementary Figure 3. (a) Photoluminescence spectra of NC1 at the excitation wavelength 410nm and emission at 635nm. (b) PL spectra of intracellular PpIX generated by NC1, two different cell lines (red line MKN-74, orange line C6) after treatment of NC1 (1mg/mL) for 6 hours.

Supplementary Figure 4. The standard curve fit of Bicinchoninic acid (BCA) protein assay

Supplementary Figure 5. Cytotoxicity test on six cells after being incubated with various concentration of NC1 for 6h, 12h and 24 h respectively, as determined using CCK-8 assays.

Supplementary Figure 6. Morphological differences at two cell types, (a) 3T3-L1 (fibroblast cells) (b) MKN-74 (gastric adenoma) (c) the morphologies of mixed cells in a co-culture microenvironment after 24 hours being seeded with different seeding ratio

Supplementary Figure 7. Fluorescence images of selective turn on fluorescence signals generated by nanocarriers in a co-culture condition with the mixture of MKN-74 cells and 3T3-L1 cells.

Supplementary Figure 8. Fluorescence images of selective turn on fluorescence signals generated by nanocarriers in a co-culture condition with the mixture of MKN-45 cells and human fibroblast cells.

Supplementary Figure 9. Fluorescence images of selective turn on fluorescence signals generated by nanocarriers in a co-culture condition with the mixture of C6 cells and MKN-74 cells.

Supplementary Figure 10. IVIS Images of mice. All mice were conducted by repeated injection of nanocarrier and time-dependent imaging in day 3 and day 14 respectively.

Supplementary Figure 11. Fluorescence immuno-labeling analysis. A representative microscopy image of sectioned tumors, illustrating localization of Nuclei (DAPI; blue), CD44 (green), CD31 (blue).

Chapter 1. Introduction

Nanoparticle-based bioimaging technologies have received a wide attention in biomedical fields for several decades.¹⁻⁶ Innovative development of novel fluorophores plays a key role for clinical success.⁷⁻¹¹ However, inevitable issues relating safety and efficacy are always accompanied in clinical trial. Moreover, good manufacturing practices (GMPs) including scaling-up, manufacturing processes, Food and Drug Administration (FDA) guidelines should be critically taken account for commercialization perspectives.¹²⁻¹⁴ Therefore, most nanoparticle-based bioresearch stays at preclinical status not exceed the hurdles of clinical barriers. An unprecedented approach is absolutely required for clinical and practical use. Here, we introduce a new paradigm of selective cancer targeting like a lighthouse. To achieve selective navigating by fluorescence,^{15,16} we have designed targeting nanocarriers containing natural fluorescent precursor. Most importantly, all the materials used in this study have already been approved for clinical use.¹⁷⁻²³ Finally, no chemistry such as covalent conjugation acting as a big barrier to clinical approval has been used during the preparation of nanoparticles. We have demonstrated selective targeting of cancer cells (including in vivo xenograft models) and targeted “turn-on” fluorescence upon delivery of nanocarriers to achieve excellent sensitivity with high signal-to-noise ratio. Owing to the non-toxic and

distinct fluorescence, we expect that our nanocarriers developed in this study will be 'extremely fast' to be exploited for clinical use.

Chapter 2. Experimental details

2.1 Materials

All chemical reagents were purchased from commercial suppliers and used as received without further purification steps.

2.2 Preparation of nanocarriers encapsulating 5-ALA

A refined soybean oil was purchased from Sigma. Hyaluronic acid (Research grade from Lifecore, MW = 91-175 kDa). 5-aminolevulinic acid (5-ALA) were purchased from Sigma. Sorbitan monoesters (Span 80), Polyethylene glycol 20 (PEG-20) sorbitan monooleate (Tween 80) technical grade - suitable for cell culture - purchased from Sigma. By adjusting the Span to Tween ratio, various HLB (hydrophilic-lipophilic balance) values can be achieved allowing the emulsification of many industrial raw materials. The mixed HLB value of co-surfactants was derived by multiplying HLB values of Span 80 and Tween 80 with their weight fractions. The oily phase (Soybean oil) containing co-surfactant, which is the mixture of Span80 and Tween80, the aqueous phase (Sodium hyaluronate and 5-ALA) were prepared separately in glass vials. The nanocarrier was prepared using soybean oil, co-surfactants and aqueous phase in the weight ratio of 7:1:2. The entire solution including soybean oil, co-surfactants and aqueous phase (1wt% Hyaluronic acid and 1, 3, 5wt% 5-ALA, respectively) was

mixed thoroughly in a glass vial using vortex for 30 seconds. The mixture solution was ultrasonicated using 6mm probe tip-sonicator at amplitude 40% (Sonics, VC-750) for 10 mins without on-off pulse cycles. After ultrasonication, the mixture's bluish color was become transparent (or translucent). To separate the nanocarriers from oily phase, the resulting oily solution was re-dispersed in DI water to separate nanocarriers from the oil phase followed by the same procedure of ultrasonication. The water phase containing nanocarriers was carefully collected was filtered through a single-use filter cartridge (Cellulose acetate syringe filter, model DISMIC-13 from Advantec). Finally, dialysis step was performed using a dialysis membrane (molecular weight cut off 1kDa) to remove other small molecules suspended in solutions for 24 hours.

2.3 Physicochemical Characterization and Stability Monitoring

The mean size, distribution and zeta potential were determined using Zetasizer Nano (Malvern, Westborough, MA). Measurements were carried out with a scattering angle of 173° and at a constant temperature (25 °C). The morphology of nanocarriers was characterized by transmission electron microscopy (HR-TEM, JEM-3010, Japan). The TEM samples were prepared by drying a droplet of the nanocarrier suspension on 400 mesh-size carbon film-coated copper grid (Ted Pella

Inc.) Then the grid was placed on the drop of 2% (w/v) sodium phosphotungstate solution for negative staining. Based on the TEM images, the size distribution data was obtained by counting over 190 particles. The stability of nanocarriers was monitored by measuring the size for six months at different time intervals, wherein the nanocarrier's solution (concentration : 1mg/mL) were stored at 4 °C in deionized (DI) water.

2.4 Determination of Entrapment ratio of 5-ALA

For the determination of 5-ALA contents entrapped into the spherical nanocarrier, it was determined according to the comparative analytical method using a 2,4,6-trinitrobenzene sulfonic acid (TNBS) kit (Thermo fisher). The primary amine group in 5-ALA was quantified, after the nanocarrier's solution (1mg/mL) was entirely lyophilized. The total amount of 5-ALA contents in 1mL of the solution was estimated based on the standard linear curve-fitting. (Figure supplementary data)

2.5 Degradation Test by hyaluronidase (HAase)

To confirm the effect of degradation by enzyme, the degradation of nanocarriers by hyaluronidase (HAase, Sigma) was tested. At first, the nanocarrier's solution (1 mg/mL) was monitored by measuring the hydrodynamic size at for 24 hours, which was stored at 4 °C and 37 °C in deionized (DI) water and PBS buffers and (pH 6.5 and 7.4, respectively). And then

50 units/mL of HAase was added to each solution and the stability was repeatedly checked.

2.6 Cell culture

For in vitro assays, six different type of cell lines was used: gastric cancer cell lines, brain cancer cells lines and fibroblast cell lines. The human gastric adenocarcinoma cell lines MKN-45 and MKN-74, the human glioblastoma U87-MG, the mouse fibroblast cell line 3T3-L1, and the mouse glioma cell line C6, were obtained from Korean Cell Line Bank (Seoul, Korea). The human fibroblast (HF) was thankfully provided by prof. Hur at Seoul National University Bundang Hospital. MKN-45, MKN-74 and C6 cells were cultured in RPMI 1640 supplemented with 10% Fetal bovine serum (FBS) and 1% antibiotic (penicillin-streptomycin). U87-MG and HF were cultured in DMEM supplemented with 10% FBS and 1% antibiotic (penicillin-streptomycin). 3T3-L1 was culture in DMEM supplemented with 10% bovine calf serum (BCS) and 1% antibiotic (penicillin-streptomycin). All cell lines were incubated in a humidified 5% CO₂ incubator at 37°C.

2.7 Fluorescent imaging of Cellular uptake and Receptor blocking assay

For fluorescent microscope imaging, all cells were prepared for each condition and the cells at a density of 1×10^4 /well were

cultured on 24-well plate at 37 °C in a humidified incubator with 5% CO₂ for 24 h. Then, washing twice with PBS, the medium was replaced by the serum-free medium containing nanocarriers (the final concentration 0.1 mg/mL) with the maintenance at 37 °C in a humidified environment with 5% CO₂ for another 1, 3 and 6 hours. Subsequently, the cells were washed twice with PBS to remove nanocarriers. For fixed cell imaging, the cells were treated with 200 mL 4% paraformaldehyde(PFA) solution for 10 min. The nuclei were stained with 4', 6-diamidino-2- phenylindole (DAPI) (Sigma) for 3 min and then, F-actin was stained with phalloidin-AlexaFluor488 (Invitrogen) for 5min. Finally, the cells were viewed under fluorescent microscope. For CD44 blocking assay, before 1 hour to treat nanocarriers, the medium was replaced with serum-free medium containing free HA polymer (the final concentration 10 mg/mL) to block the CD44 receptors after washing twice with PBS, then followed by the same treatment of nanocarriers' uptake assay for 3 h as described above.

2.8 Flow cytometry analysis

All cells were cultured via the same procedures described above, then the cells at a density of 5×10^4 /well were cultured on 35 mm cell culture dish at 37 °C in a humidified incubator with 5% CO₂ for 24 h. Then, washing twice with PBS, the

medium was replaced by the serum-free medium containing nanocarriers (the final concentration 0.1 mg/mL) with the maintenance at 37 °C in a humidified environment with 5% CO₂ for 3 h. To demonstrate receptor blocking experiments as a control group, the same procedure was also carried out, described above but the pretreatment of free HA polymer was to block the CD44 receptors. Subsequently, after 3 hours, the cells were washed twice with PBS to remove nanocarriers. The remaining cells were trypsinized and re-suspended in 5 mL of PBS solution. After centrifugation, the cells were suspended in 0.5 mL PBS solution, followed by flow cytometry analysis. The analysis was performed on a flow cytometry device (BD FACS Aria II flow cytometer, BD Biosciences).

2.9 The quantification of PpIX fluorescence induced by 5-ALA NCs

The generation of PpIX was quantified in each cell line by the adjusted method. Briefly, all prepared cells were cultured on 24-well plate in a humidified incubator with 5% CO₂ at 37 °C. After replacing the serum-free media containing nanocarriers (the final concentration was 0.1 mg/mL), the cells were lysated with 100µL of RIPA lysis and extract buffer (Biosesang) at each time point (0.5, 1, 2, 3, 4, 6, 12 and 24 h) and the extracted solution were transferred into black 96-well plate. Especially, after incubating 4 hours later the media was

changed to fresh serum-free media to eliminate the effect of nanocarriers. Next, the fluorescence intensity was measured at 410 nm excitation and 635 nm emission using a microplate reader on the fluorescence detection mode (Synergy H1, BioTek). To correct for the absolute fluorescence value in cell numbers, the fluorescence intensities were adjusted by proteins extracted from the cells, wherein the protein concentration of each cell line was estimated based on bicinchoninic acid (BCA) assay (Thermofisher) (Figure supplementary data)

2.10 Cytotoxicity

All cells were cultured on 96-well plate for in vitro cytotoxicity screening in a humidified incubator with 5% CO₂ at 37 °C. The effect of nanocarriers on cell viability was carried out using the cell counting kit 8 (CCK-8) (Dojindo Lab, Tokyo, Japan). Briefly, all cells were seeded in 96 well plates at a density of 5×10^3 cells/well. After pre-incubation for 24 hours, cells were treated with various concentrations of nanocarriers (0.062, 0.125, 0.25, 0.5, 1 and 2 mg/mL) for 6 h, 12 h and 24 h at 37°C, respectively. Cells cultured in the medium without adding nanocarriers served as a negative control group. At the end of the treatment, CCK-8 solution was added to each well and the plates were incubated for 2 h at 37 °C. The optical density (OD) of each well at 450 nm was recorded on a microplate reader (Synergy H1, BioTek).

2.11 Cancer-selective targeting in co-culture models

To evaluate selective uptake in three types of co-culture models[ref](C6/MKN-74, 3T3-L1/MKN-74 and HF/MKN -45), all cells were incubated at the same condition described above. Each mixture of cells with different ratio from 1:1 to 1:10 were seeded onto 24 well plates with different total number of cells per well (Low : 5×10^4 /well, Mid : 1×10^5 /well and High : 2×10^5 /well). The mixture of C6/MKN-74 cells were cultured in RPMI 1640 supplemented with 10% FBS and 1% antibiotic (penicillin-streptomycin). The mixture of 3T3-L1/MKN-74 cells were cultured in DMEM supplemented with 10% BCS and 1% antibiotic (penicillin-streptomycin). The mixture of HF/MKN-45 cells were cultured in DMEM supplemented with 10% FBS and 1% antibiotic (penicillin-streptomycin). After 12 hours pre-incubation, these cells were replenished with medium containing nanocarriers (final concentration 0.1mg/mL) and incubated for 1, 2, 3 and 6 hours, receptively. After washing in PBS twice, the same processes ware performed to fixation, DAPI staining and F-actin staining, and then each wells were sealed using a round cover glass to prevent the wells from drying. And every cells were visualized by fluorescence microscopy and representative photographs were obtained.

2.12 Fluorescent Live-cell Imaging

For the live-cell images, the MKN-74 cells and the co-cultured cells (MKN-74/3T3-L1) were prepared for each condition described above at the total density of 5×10^4 /mL on the Confocal Cell Imaging 35 mm Dish for 24 hours. The nuclei were stained with 4', 6-diamidino-2-phenylindole (DAPI) (Sigma) for 3 min and then, after washing twice with PBS, the serum-free medium containing nanocarriers (final concentration 0.1 mg/mL) was filled up. The real-time fluorescent live-cell images were obtained using the fluorescent microscope, equipped with the live-cell incubating chambers at 37 °C with 5% CO₂ for 6 hours with a time interval of 5 mins. The time-lapse images were analyzed and exported to video files using the Zeiss Zen II software.

2.13 Animal studies

Mouse breeding was conducted in the Laboratory Animal Resources facility of WOOJUNGBSC., Co. LTD. (Suwon, Korea), housed in a 12 hours day and night cycle, with supplying adequate food and water. All animal experiments complied with the guidelines by Institutional Animal Care and Use Committee (IACUC). Six to eight-week-old male athymic Balb/c mice were purchased from Orient Biotech (Seoul, Korea). The athymic nude mice were inoculated with fibrin gel subcutaneously over the right forelimb armpit by injection of MKN-45 cells (1×10^7). To determine the best condition for

inoculation before the entire gelation, fibrinogen from bovine plasma (Sigma) containing the cell pellet and thrombin from bovine plasma (Sigma) mixed with optimal concentrations to the sol/gel transition in 10–15 seconds. After inoculation (day 3 and day 14, respectively) the nanocarriers (1 mg/mL injection of 100 μ L volume) were repeatedly injected subcutaneously into the same mice via the same method to deliver nanocarriers locally. Additionally, 5-ALA molecules were injected into the same mouse models as other control groups. The injected concentration of 5-ALA (50 μ g/mL) were determined based on the result, characterized by the entrapment of percentages. Fluorescence imaging was performed at 0, 20, 40, 60, 120, 180, 240 mins and 24 hours post-injection by using In Vivo Imaging System (IVIS Lumina XRMS, Perkin Elmer, CLS136340). The fluorescence signals were acquired on the condition of 420/20 nm excitation and 620/40 nm emission filter.

2.14 Immunofluorescence assay

In order to access the expression level of CD44 and CD31, the resected tumors were immunostained according to standard immunofluorescence protocols with the appropriate antibodies: anti CD31 antibody (rat anti-mouse, BD Pharmingen 553370), alexa fluor 594 goat anti-rat IgG (H+L) antibody (Life Technologies, A-11007) and anti-CD44-FITC antibody (rat anti-mouse, eBioscience, 11-0441-82). Prior to microscopy, the

nuclei were counter-stained. The stained slides were visualized by fluorescence microscopy.

2.15 Survival rate and Weight variation

In order to monitor the concentration-dependent survival rate and its consecutive weight variation, 21 mice were randomly divided into three groups (seven in each group), and injected nanocarriers of different concentration (1, 3 and 5 mg/mL, respectively). Mice received intravenous administration volume of approximately 100 μ L nanocarriers' solution. Once a week, four injections were given to each group, and the body weight of mice in each group was tracked along the survival study, then mice were sacrificed after 28 days from the first injection of nanocarriers.

Chapter 3. Result and Discussion

Nanocarriers were mainly comprised of hyaluronic acids (HAs). HAs provide not only skeletal structures of polymeric nanocarrier but also act as anti-CD44 membrane epitopes overexpressed in most cancer cells. Non-fluorescent 5-aminolevulinic acid, (5-ALA) known to be transformed to a fluorescent moiety through biosynthesis pathway in cells has been physically incorporated in HA nanocarriers. Once being delivered in cancer cells by receptor-mediated endocytosis, the nanocarriers would turn on distinctive fluorescent light as shown in **Figure 1. a**. Cancer cells can be selectively lighted on by excitation, showing the distinguishable light themselves. We have achieved significant enhancement of sensitivity by minimizing fluorescence background. Furtherly, we have demonstrated novel approaches to in-vitro culture models and in-vivo local delivery methods to evaluate the selectivity of our nanocarriers.

The nanocarriers were manufactured through simple two steps, water-in-oil (W/O) emulsification and phase transfer technique. (**Supplementary Figure 1. a.b.**) After the W/O emulsification, a large amount of particles was trapped within oily phase. By simply transferring the entrapped particles to water phase, homogenous particles in large quantities were obtained, which showed excellent stability for more than six-months (**Figure 1. b.**). The size range of carriers, measured by transmission

electron microscopy (TEM), which displayed a spherical shape, indicated the average size 53.58 nm (**Figure 1. c.**). In addition, the result is corroborated by dynamic light scattering (DLS) (**Supplementary Figure 1. c.**). The characterization results of three nanocarriers (size, zeta potential, and 5-ALA entrapment ratio) are summarized in table 1.

To verify release of 5-ALA encapsulated inside the carriers' structure in the cells, we performed the enzymatic degradation test,²⁴ assuming the effect on hyaluronidase (HAase) (**Figure 1. d.**). The nanocarrier stably maintained for 24 hours under different conditions began to be affected by the HAase within 4 hours. This clearly demonstrates the effect of HAase. The nanocarrier was physically entangled with anionic HA polymer and 5-ALA and partial interaction through ionic bonding; thus, cleavage of HA polymer chains resulted in nano-sized spherical structure could be broken down, then entrapped 5-ALA to be released to the cytoplasm. The percentage of 5-ALA entrapped inside nanocarriers varied around 5 - 10 %, (**Supplementary Figure 2.**). Once the nanocarriers are specifically enabled CD44 receptor-mediated endocytosis, subsequently enzymatic degradation in lysosomes occurs.^{17,24,25} The high stability in the aqueous solution and the property of enzymatic degradation make nanocarriers ideal to be stored for long-term and for the usage. The nanocarrier had not any fluorescence signals. However, after internalization to cells through RME, released

5-ALA by the enzymatic degradation can be converted into PpIX. (**Figure 1. a., Supplementary Figure 3.**) This specific mechanism is well known as the pathway of heme biosynthesis.²¹

To determine whether the nanocarriers can be selectively targeted to cancer cells, we examined in vitro uptake assay on six cell lines. After 6 hours of incubation with nanocarriers, the normal fibroblast cell lines displayed any fluorescent change on the microscope images. (**Figure 2. a.b.**) On the other hand, we observed fluorescence signals gradually appears after uptake 3 hour in four cancer cells, (**Figure 2. c-f.**) suggesting specificities of nanocarriers. Furthermore, if the CD44 receptor of the cells was blocked, fluorescence intensity could not be observed after uptake 3 hour even in cancer cells. The cell uptake suggested by fluorescence microscopy was confirmed by flow cytometry experiments. (**Figure 2. g.**) These data not only demonstrated nanocarriers was efficiently delivered to targeted cells, mediated the CD44 receptor, but also suggested that cancer cells were visualized through fluorescent turn on signals.

In order to measure fluorescence intensity quantitatively, the value of fluorescence intensity, which is proportional to the number of cells, was adjusted. For adjustment, PL intensity value was corrected based on the amount of cell's protein analyzed by the bicinchoninic acid (BCA) assay. (**Supplementary Figure 4.**) The adjusted result shown in

Figure 2. g. revealed that the fluorescence signals dramatically increase in cancer cells compared to normal cells. To check whether the result is affected by nanocarriers, after 4 hours the media was replaced to serum-free media without nanocarriers. From this point, the signals gradually decreased because of natural degradation.

The substance constituting the nanocarrier are non-toxic materials, viability assays (CCK-8) are performed to determine the cytotoxicity of nanocarriers in proportion to the concentration and the time (**Supplementary Figure 5.**) Nanocarriers mainly comprised of two natural components, HA and 5-ALA, which already exists in the body, thus they can be naturally degraded; Even if the cells were introduced at a high concentration, non-toxic effect was confirmed.

In real tumor microenvironment, cancer cells were surrounded by various cells such as fibroblasts, adipocytes, endothelial cells with extracellular matrix (ECM) components.^{26,27} We studied in vitro co-culture selective navigation models²⁸ to evaluate whether the actual targeting is possible to cancer cells surrounded by normal cells. (**Figure 3. a.**) Regarding cell morphologies, MKN-74 cells have a tendency to agglomerate, while the spreading pattern of fibroblasts, which show a typical spindle-shape morphology, is different; thus we hypothesized the effect of nanocarriers can be distinguished based on the phenotypic traits. (**Supplementary Figure 6.**)

Interestingly, in a cancer/normal cells environment (MKN-74/3T3-L1), we observed that agglomerated cells gradually emitted fluorescence signals. (**Figure 3. b.**) This result indicated the targeted efficiency of nanocarriers and selective turn on fluorescence signals. In addition, at low resolution of microscope image, the agglomeration of MKN-74 cells showed distinguishable strong fluorescence signals without background noise. (**Figure 3. c.**) Regardless of the number of fibroblast cells near MKN-74 cells and the total number of cells seeded on the dish, the same result was obtained. (**Figure 3. d., Supplementary Figure. 7.**) An additional examination co-cultured in cancer/normal cells (MKN-45/Human fibroblast) corroborated the selectivity to cancer cells. (**Supplementary Figure. 8.**) On the contrary, fluorescence signals appeared on all cells over time in a cancer/cancer cells environment (C6/MKN-74) (**Supplementary Figure. 9.**). Taken together, the results demonstrated nanocarriers' targeting efficiency is excellent even in a co-culture environment.

Our goal is to selectively turn on targeted cancer lesions in vivo; Accordingly, experimental procedures were designed for repeated injection locally around the tumor site. (**Figure 4. a.**) After MKN-74 cells inoculation, the time interval of injection was set sufficiently to eliminate nanocarriers' effects on mice. The merit of turn on signals holds the potential to minimize background noise, which would result in much higher

sensitivity.^{4,29} As depicted in **Figure 4. b.**, if fluorescence signal was only turned on tumor lesions, it will make signal-to-noise ratio maximized. After nanocarrier injection locally, as expected, strong fluorescent signals on tumor inoculated lesions gradually turned on. (**Figure 4. c. Supplementary Figure. 10.**) Particularly, we observed that fluorescence intensity between 3 and 4 hours was maximized. By contrast, all mice in the controls, administration of free 5-ALA, showed non-distinctive fluorescence features. In fluorescence immuno-labeling analysis, expression of CD44 and CD31 were confirmed in the resected tumor section. (**Supplementary Figure. 11.**)

During the experiment for repeated local injection, all mice could survive without any changes in physical activity. As potential toxicity is fundamentally important, we evaluated the toxicological test via intravenous (i.v.) administration of nanocarriers in tumor-free healthy mice. Even if administrated up to the higher concentration five times than that of IVIS image, all mice were not affected by nanocarriers (**Figure 4. d.e.**) Nanocarriers proved to have no toxic effect, as same to the in vitro result.

5-ALA is already FDA approved for clinical application.¹⁰ However, its clinical use is limited to malignant tumor resection (such as glioma and glioblastoma in WHO grade III and IV), but little is known on its delivery and accumulation mechanism. Most prevalent and widely accepted hypothesis suggested the

enzyme configuration in malignant cells but, these are still open for debate.^{21,30}

Instead, our study aims to validate selective delivery of 5-ALA via nanocarrier rather than to support either of the hypothesis above. Zwitterionic 5-ALA alone does not harbor selectivity to cancer cells for lack of targeting moiety, and are not permeable to lipid bilayer. Therefore, certain researches have reported in vitro targeted delivery via chemical conjugation of PpIX precursor to targeting moiety.³¹ We present selective internalization to cancer cells which are substantiated by the data where anti-CD44 moiety carry RME internalization and releases 5-ALA in cytoplasm. Regardless of current controversy on PpIX accumulation to cancer cells, if nanocarriers successfully delivers 5-ALA to cancer cells, this accumulated fluorescence feature would be the phenomenal advantage.

Furthermore, our results of co-culture targeting model demonstrates remarkable selectivity of nanocarrier, though it would not be negligible to cell-to-cell communication, cytokine, and other biological factors in a co-culture environment.²⁷ However, our methods offer a novel strategy beyond conventional in vitro testing targeting efficiency only for single cell lines. In addition to in vitro models, Certain scientists also questions efficacy and validity of nanomaterials in animal in vivo models (e.g. EPR effect). More research needs to be done to validate which animal model is most adequate and ideal in

tumor targeting study. We expect our work can present a perspective for next generation imaging agents. There are plenty of room for future research such as fluorescence based surgical diagnosis, precise tumor resection and cytoreductive treatment.

Chapter 4. Conclusion

This study described the design of a new polymeric nanocarrier, encapsulating fluorophore precursors. Our approach to fabricate nanocarrier is very simple to mass-produce. The nanocarrier is highly stable, which lead to qualify long-term storage and reduce manufacturing cost. Most importantly, the results of both in vitro and in vivo studies demonstrated non-toxicity, targeting efficiency (selectivity), and selective navigating turn on signals (sensitivity). Therefore, our strategies are expecting to escape the addressed issues in the field and will be extremely fast to be exploited for clinical use. Future works will focus on demonstrating in vivo surgical accurate resection as well as striving to extend cytoreductive treatment with photodynamic therapy to prevent tumor recurrence.

References

1. Weissleder, R., Tung, C.H., Mahmood, U. & Bogdanov, A., Jr. In vivo imaging of tumors with protease-activated near-infrared fluorescent probes. *Nature biotechnology* 17, 375-378 (1999).
2. Terai, T. & Nagano, T. Fluorescent probes for bioimaging applications. *Current opinion in chemical biology* 12, 515-521 (2008).
3. Olson, E.S. et al. Activatable cell penetrating peptides linked to nanoparticles as dual probes for in vivo fluorescence and MR imaging of proteases. *P Natl Acad Sci USA* 107, 4311-4316 (2010).
4. Weaver, J.B. Bioimaging: Hot nanoparticles light up cancer. *Nature nanotechnology* 5, 630-631 (2010).
5. Kotov, N. Bioimaging: The only way is up. *Nature materials* 10, 903-904 (2011).
6. Yao, J., Yang, M. & Duan, Y. Chemistry, biology, and medicine of fluorescent nanomaterials and related systems: new insights into biosensing, bioimaging, genomics, diagnostics, and therapy. *Chemical reviews* 114, 6130-6178 (2014).
7. Hwang, S.W., Malek, A.M., Schapiro, R. & Wu, J.K. Intraoperative Use of Indocyanine Green Fluorescence Videography for Resection of a Spinal Cord Hemangioblastoma. *Neurosurgery* 67, 300-302 (2010).
8. Choi, H.S. et al. Targeted zwitterionic near-infrared

fluorophores for improved optical imaging. *Nature biotechnology* 31, 148–153 (2013).

9. Ishizuka, M. et al. Intraoperative Observation Using a Fluorescence Imaging Instrument during Hepatic Resection for Liver Metastasis from Colorectal Cancer. *Hepato-Gastroenterol* 59, 90–92 (2012).

10. Vahrmeijer, A.L., Hutteman, M., van der Vorst, J.R., van de Velde, C.J.H. & Frangioni, J.V. Image-guided cancer surgery using near-infrared fluorescence. *Nat Rev Clin Oncol* 10, 507–518 (2013).

11. Schnermann, M.J. Chemical biology: Organic dyes for deep bioimaging. *Nature* 551, 176–177 (2017).

12. Zhang, R.R. et al. Beyond the margins: real-time detection of cancer using targeted fluorophores. *Nat Rev Clin Oncol* 14, 347–364 (2017).

13. Bobo, D., Robinson, K.J., Islam, J., Thurecht, K.J. & Corrie, S.R. Nanoparticle-Based Medicines: A Review of FDA-Approved Materials and Clinical Trials to Date. *Pharmaceutical research* 33, 2373–2387 (2016).

14. Eifler, A.C. & Thaxton, C.S. Nanoparticle therapeutics: FDA approval, clinical trials, regulatory pathways, and case study. *Methods in molecular biology* 726, 325–338 (2011).

15. Van Dam, G.M. et al. Intraoperative tumor-specific fluorescence imaging in ovarian cancer by folate receptor- α targeting: first in-human results. *Nature medicine* 17, 1315

(2011).

16. Uchiyama, K. et al. Combined use of contrast-enhanced intraoperative ultrasonography and a fluorescence navigation system for identifying hepatic metastases. *World journal of surgery* 34, 2953–2959 (2010).

17. Toole, B.P. Hyaluronan: from extracellular glue to pericellular cue. *Nature reviews. Cancer* 4, 528–539 (2004).

18. Ahrens, T. et al. Soluble CD44 inhibits melanoma tumor growth by blocking cell surface CD44 binding to hyaluronic acid. *Oncogene* 20, 3399 (2001).

19. Dufay Wojcicki, A. et al. Hyaluronic acid-bearing lipoplexes: physico-chemical characterization and in vitro targeting of the CD44 receptor. *Journal of controlled release : official journal of the Controlled Release Society* 162, 545–552 (2012).

20. Lee, Y. et al. Bioinspired surface immobilization of hyaluronic acid on monodisperse magnetite nanocrystals for targeted cancer imaging. *Advanced Materials* 20, 4154–4157 (2008).

21. Ismail, M.S. et al. Modulation of 5-ALA-induced PpIX xenofluorescence intensities of a murine tumour and non-tumour tissue cultivated on the chorio-allantoic membrane. *Lasers in medical science* 12, 218–225 (1997).

22. Eickhoff, A. et al. Long-Segment early squamous cell carcinoma of the proximal esophagus: curative treatment and

- long-term follow-up after 5-aminolevulinic acid (5-ALA)-photodynamic therapy. *Endoscopy* 38, 641-643 (2006).
23. Kaneko, S. & Kaneko, S. Fluorescence-Guided Resection of Malignant Glioma with 5-ALA. *International journal of biomedical imaging* 2016, 6135293 (2016).
24. Wang, J. et al. Gd Hybridized Plasmonic Au Nanocomposites Enhanced Tumor Interior Drug Permeability in Multimodal Imaging Guided Therapy. *Advanced Materials* 28, 8950-8958 (2016).
25. Jiang, T., Mo, R., Bellotti, A., Zhou, J. & Gu, Z. Gel-liposome mediated co delivery of anticancer membrane associated proteins and small molecule drugs for enhanced therapeutic efficacy. *Advanced Functional Materials* 24, 2295-2304 (2014).
26. Kessenbrock, K., Plaks, V. & Werb, Z. Matrix metalloproteinases: regulators of the tumor microenvironment. *Cell* 141, 52-67 (2010).
27. Shiga, K. et al. Cancer-Associated Fibroblasts: Their Characteristics and Their Roles in Tumor Growth. *Cancers* 7, 2443-2458 (2015).
28. Le Droumaguet, B. et al. Versatile and efficient targeting using a single nanoparticulate platform: application to cancer and Alzheimer's disease. *ACS nano* 6, 5866-5879 (2012).
29. Chan, J., Dodani, S.C. & Chang, C.J. Reaction-based small-molecule fluorescent probes for chemoselective bioimaging.

Nature chemistry 4, 973–984 (2012).

30. Walter, S. et al. Intraoperative detection of malignant gliomas by 5-aminolevulinic acid-induced porphyrin fluorescence. *Neurosurgery* 42, 518–526 (1998).

31. Han, H. et al. Intracellular Dual Fluorescent Lightup Bioprobes for Image-Guided Photodynamic Cancer Therapy. *Small* 12, 3870–3878 (2016).

Figures

Main Figures

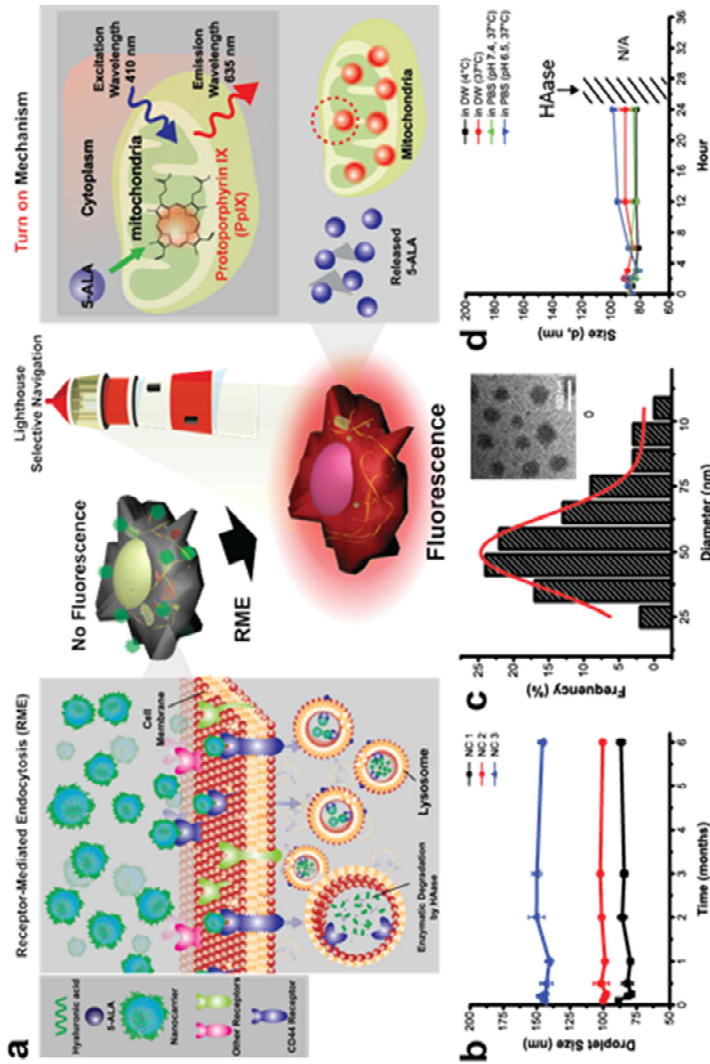


Figure 1. Schematic illustration of the lighthouse, illuminating cancer cells and selective turn on navigation, and nanocarrier (NC) physicochemical characterization. (a). nanocarriers having spherical morphologies, specific bind to CD44 receptors on the

cellular membranes which leads to cellular internalization by receptor-mediated endocytosis (RME). In cytoplasm, internalized nanocarriers encapsulated by lysosome sequentially can be degraded by the enzyme (hyaluronidase, HAase). As the polymeric structure of nanocarriers was broken, then led to release the entrapped 5-ALA to the cytoplasm. In turn, 5-ALA was converted to natural fluorescent materials, protoporphyrin IX (PpIX) in the mitochondrial biosynthetic pathway. (b). stability profiles to three different types of NCs (NC 1-3), monitored by DLS equipment for six-months, and the storage condition maintained specified for 4 °C refrigerators at equivalent concentration, 1mg/mL (c). particle-size distribution of NC1 by counting over 190 particles analyzing TEM images. The inset is a representative TEM image of NC1. Scale bar, 100nm. (d). Effect of enzymatic degradation by confirmed the size monitoring by DLS equipment. For 24 hours, NC1 stored at different conditions (DW, PBS, temperature, pH) maintained without variation in size. After treating 50 units/mL of HAase, fluctuation in size varied for a certain period of time and then the size data could not be obtained.

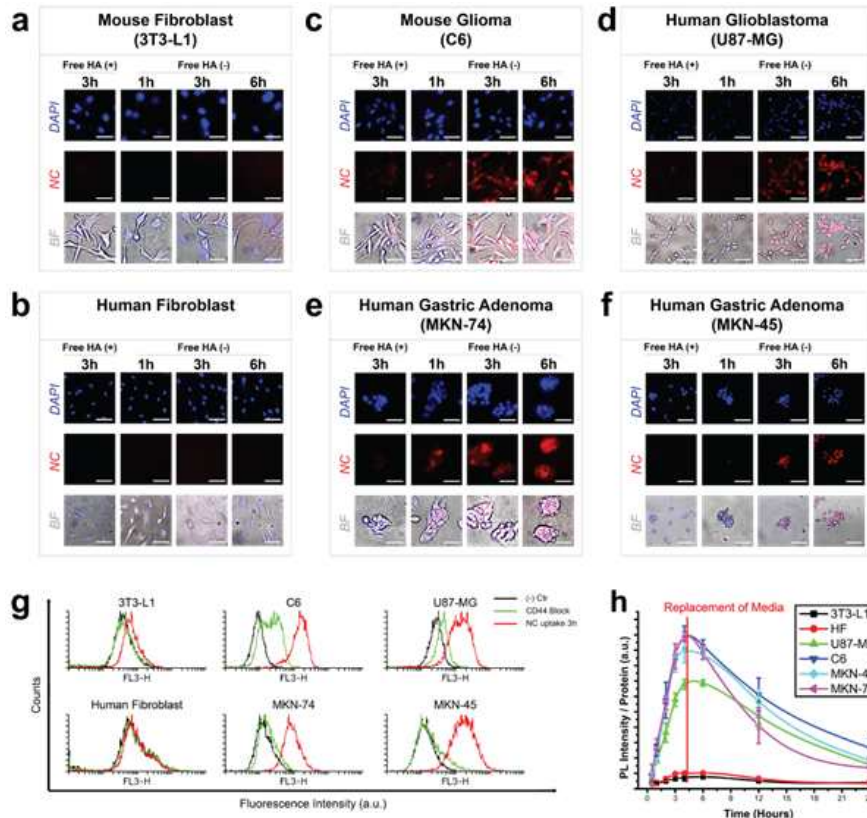


Figure 2. In vitro cellular uptake analysis to verify selective navigation of fluorescence turn on signals. (a). Mouse fibroblast (3T3-L1) (b). Human Fibroblast (HF) (c). Mouse glioma (C6) (d). Human glioblastoma (U87-MG) (e). Human gastric adenoma (MKN-74) (f). Human gastric adenoma (MKN-45). Intracellular fluorescence signal observation for 1h, 3h, and 6h, respectively: Nucleus (Dapi staining, Blue), PpIX (Red). Scale bar, 50 μ m. The observation process of fluorescence turn on signals was accessed with a fluorescence microscopy with an equivalent nanocarrier's concentration of 0.1 mg/mL. For comparison, CD44 receptor blocking study was carried out with

pretreatment 10 mg/mL of HA for 1h. After 3 hours, blocking study groups in all cell lines displayed non-fluorescence signals. (g). Flow cytometry analysis of PpIX generated by nanocarriers in six cell lines after uptake 3 hours: Non-treatment as a negative control (black line), Nanocarriers' uptake with pretreatment 10 mg/mL of HA for 1h to block CD44 receptors (green line), and Nanocarriers' uptake (red line). Uptake concentration is equivalent 0.1 mg/mL. (h). Quantification of PpIX generated by nanocarriers' selective navigation in six cell lines. The vertical axis was adjusted by the ratio (PpIX PL intensity/proteins), where the PL intensity of PpIX was measured from the lysated cells and the value of proteins in each cells were quantified by BCA assay. Red vertical line at 4 hours indicates the replacement of media cultured with nanocarriers to fresh media in order to verify the effect of nanocarrier to the PpIX generation.

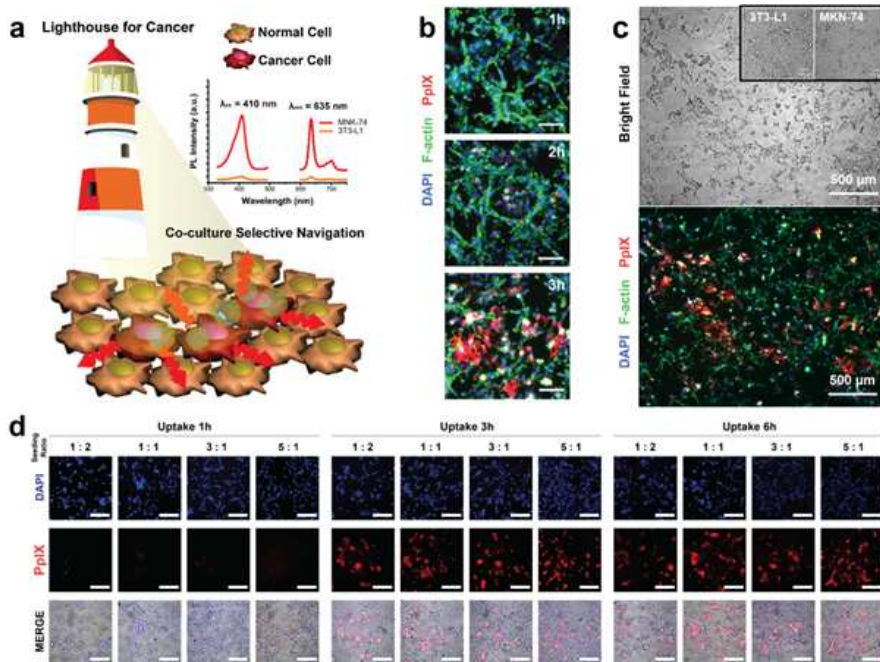


Figure 3. In vitro selective navigation in a co-culture model (a). scheme of selective navigating to cancer cells: the lighthouse for cancer illuminating fluorescence signals on specific cells toward the cell mixtures of 3T3-L1 and MKN-74. The inset represents the PL intensity obtained from the lysated cells: MKN-74 (Red line) and 3T3-L1 (Orange line), where the excitation wavelength is 410 nm and the emission wavelength 635 nm. (b). Representative merged fluorescence images of selective turn on fluorescence signals generated by nanocarriers in the co-culture condition with the mixture of MKN-74 cells and 3T3-L1 cells. The fluorescence signals were observed for 1h, 2h, and 3h, respectively. Scale bar, 100 μm . (c). Bright (upper) and merged fluorescence images at low magnification, showing the selective turn on PpIX signals on cancer cells. The

inset represents the morphologies of two cells at high density: 3T3-L1 and MKN-74, respectively, to display phenotypical differences. Scale bar, 500 μm . (d). fluorescence images to access the ability of selective navigation to MKN-74 cells surrounded by different density of 3T3-L1 cells. The seeded number of MKN-74 cells was fixed to 1×10^4 cells/well, and the seeded number of 3T3-L1 cells increased. Seeding ratio of 3T3-L1:MKN-74 varied from 1:2 to 5:1. The fluorescence signals were observed for 1h, 3h, and 6h, respectively. Nucleus (Blue), F-actin (Green), PpIX (Red).

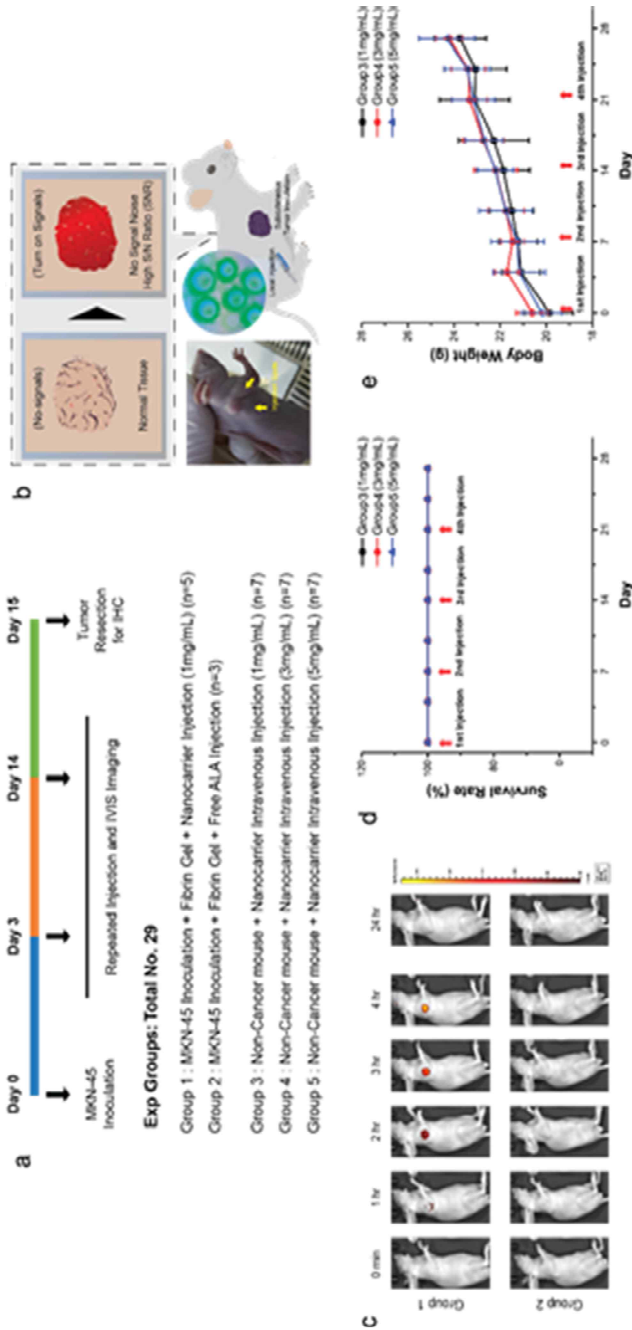
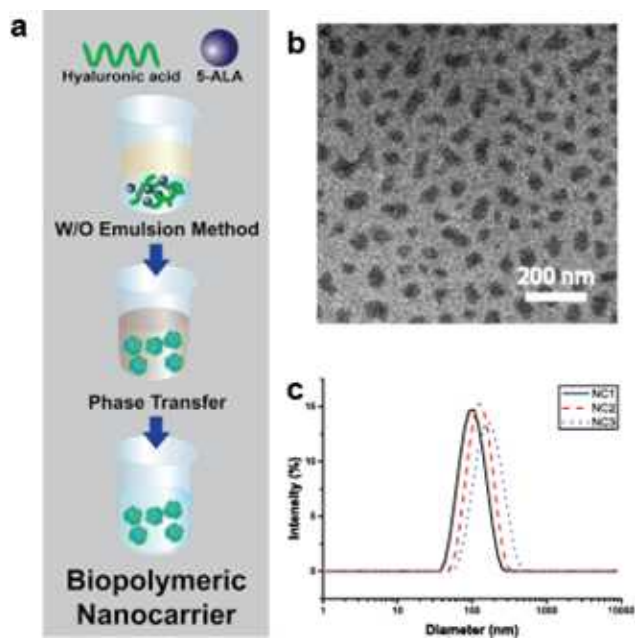


Figure 4. In vivo nanocarriers' selective navigation of turn on signals via local delivery. (a). Description of experimental design of animal studies: in vivo fluorescence imaging,

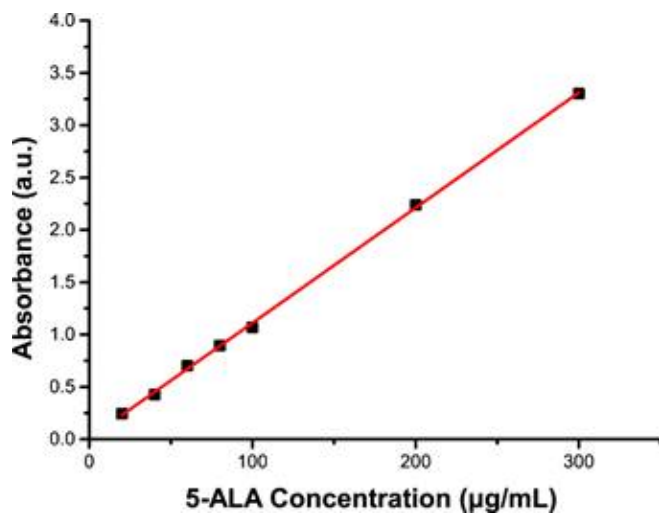
performed on four groups and in vivo toxicity test through intravenous injection performed on three groups. The total number of mice used for this research was twenty-nine. After MKN-45 tumor inoculation (1×10^7 cells), In Vivo Imaging System (IVIS) fluorescence imaging was performed 2 times repeatedly in day 3, day 14 and mice were sacrificed 24 hours after the complete degradation of nanocarriers from the last injection. Resected tumor specimens were examined in immunohistochemistry (IHC) in day 15. (b). Scheme of selective turn on signals on tumor legions, leading to maximized signals-to-noise ratio (SNR) around cancerous legions due to no signal noise. Experimental groups for fluorescence imaging were administrated with 1mg/mL of nanocarriers injected locally around the tumor site where yellow arrows indicate administration spots in the photograph of the mouse with tumor inoculated subcutaneously over the right forelimb armpit. (c). Multiple time-point in vivo fluorescence imaging via local administration in MKN-45 tumor bearing mice (Group 1, Nanocarrier administration. Group 2, Free 5-ALA administration as a control group). (d). The survival rate and body weight variation for healthy mouse to evaluate potential toxicity from nanocarriers. Twenty-one mice were randomly divided into three groups. Once a week, four repeated administrations were given to each group, and the body weight of mice in each group was tracked along the survival study. The concentration

of nanocarriers i.v. administrated were escalating up to 1x, 3x and 5x times, compared to the tumor mice model for fluorescence image.

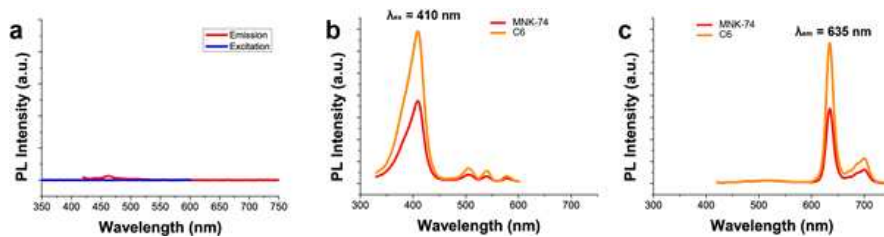
Supplementary Figures



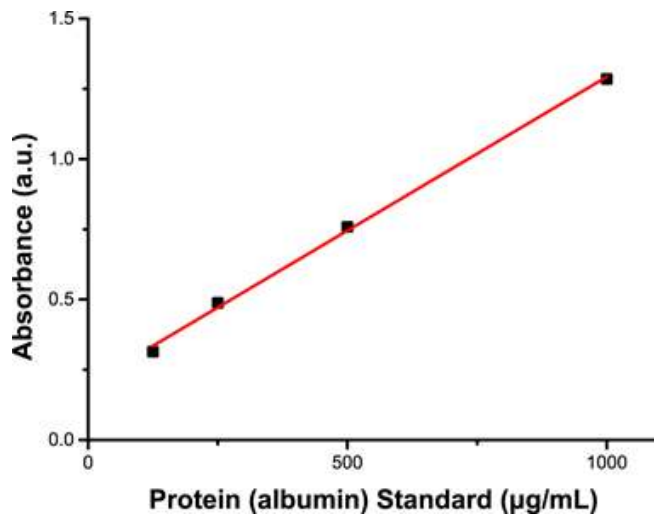
Supplementary Figure 1. (a). scheme of fabrication steps for homogenous nanocarriers, Water-in-Oil emulsification and phase-transfer from oily phase to water phase. (b) Transmission electron microscopy image of Nanocarrier 1 (NC1) at lower magnification. (c) Dynamic light histogram of NCs stored in deionized water, pH 7.4 at room temperature.



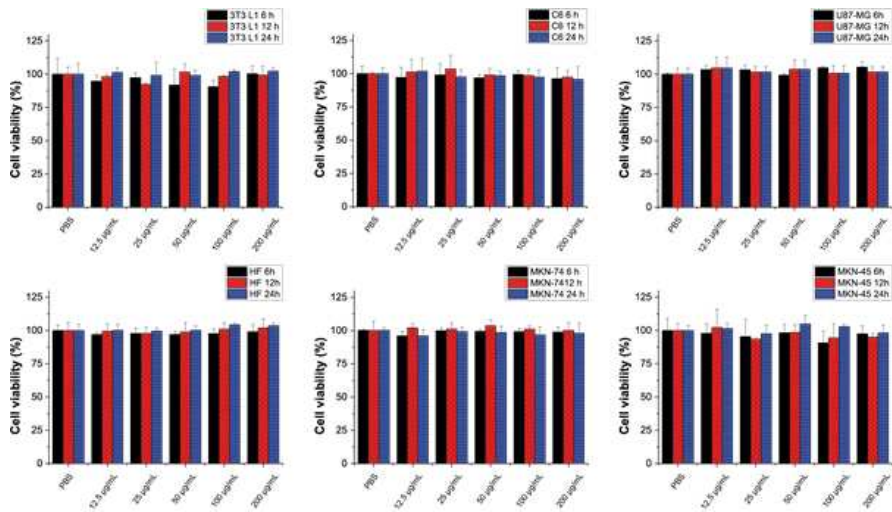
Supplementary Figure 2. The calibration curve fit of 5-ALA using 2,4,6-Trinitrobenzenesulfonic acid (TNBS) kit



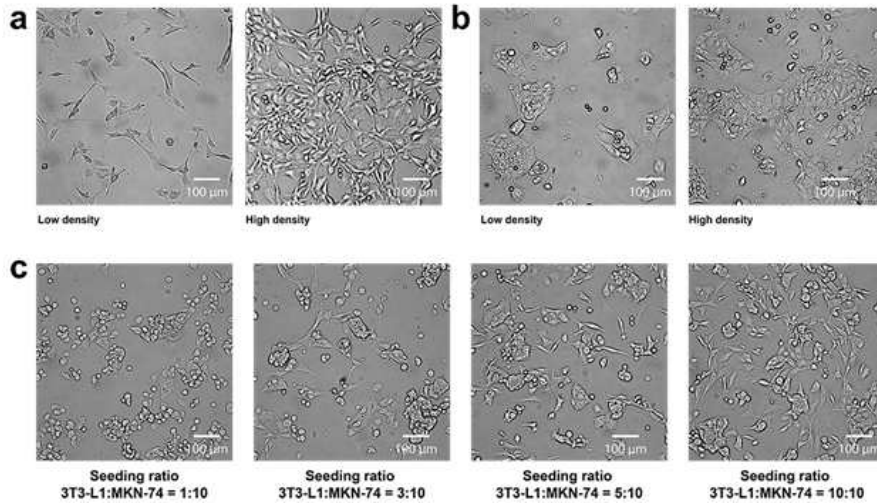
Supplementary Figure 3. (a) Photoluminescence spectra of NC1 at the excitation wavelength 410nm and emission at 635nm. (b) PL spectra of intracellular PpIX generated by NC1, two different cell lines (red line MKN-74, orange line C6) after treatment of NC1 (1mg/mL) for 6 hours.



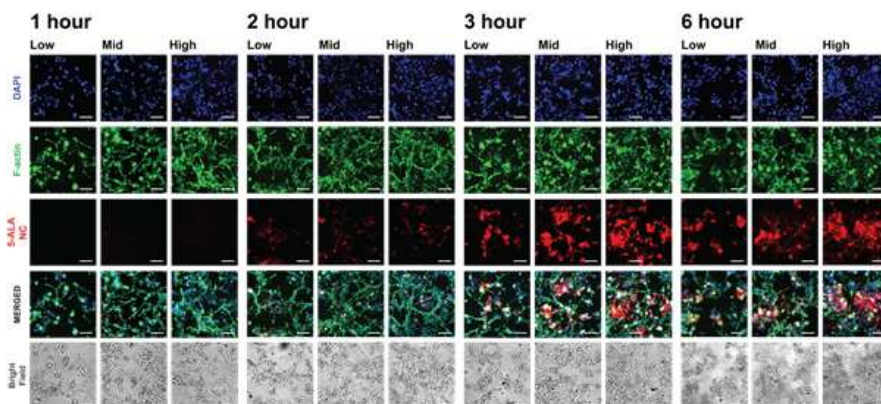
Supplementary Figure 4. The standard curve fit of Bicinchoninic acid (BCA) protein assay



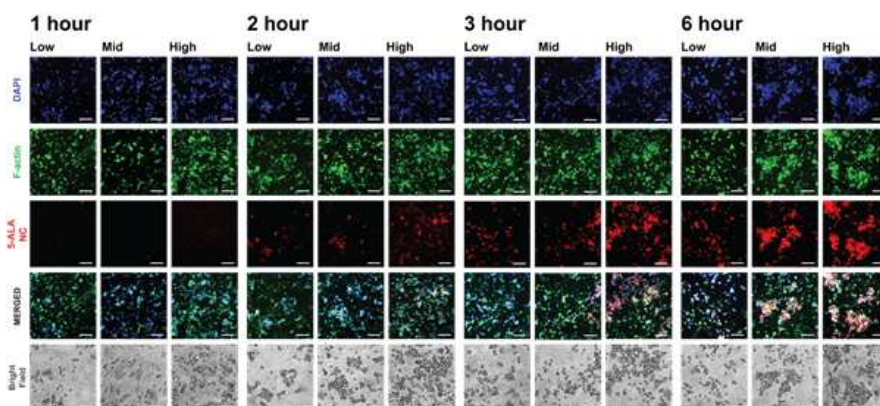
Supplementary Figure 5. Cytotoxicity test on six cells after being incubated with various concentration of NC1 for 6h, 12h and 24 h respectively, as determined using CCK-8 assays.



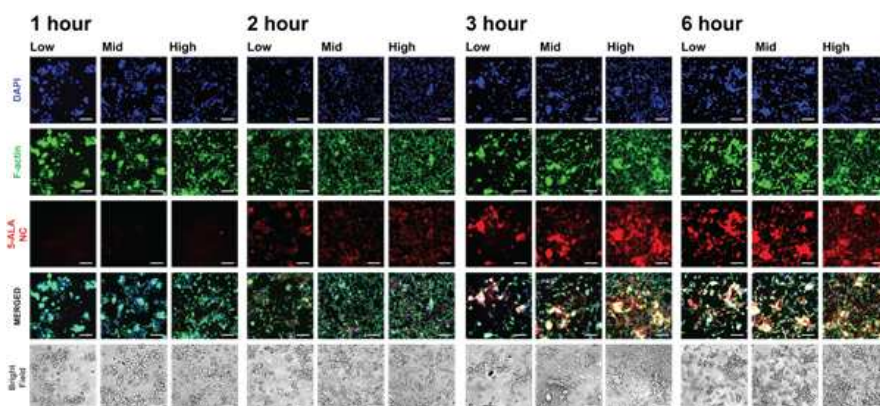
Supplementary Figure 6. Morphological differences at two cell types, (a) 3T3-L1 (fibroblast cells) (b) MKN-74 (gastric adenoma) (c) the morphologies of mixed cells in a co-culture microenvironment after 24 hours being seeded with different seeding ratio



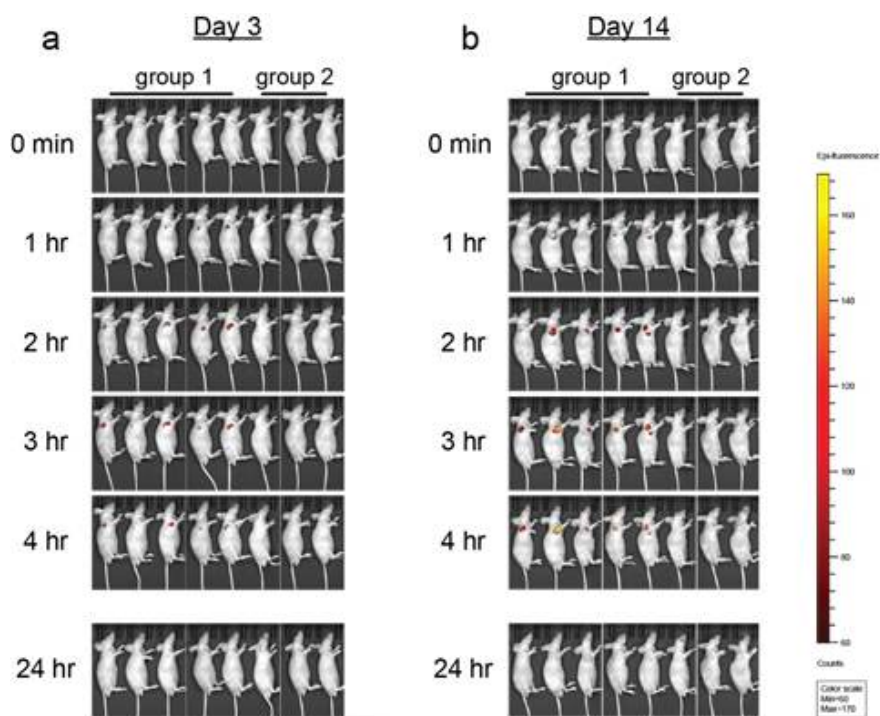
Supplementary Figure 7. Fluorescence images of selective turn on fluorescence signals generated by nanocarriers in a co-culture condition with the mixture of MKN-74 cells and 3T3-L1 cells. The fluorescence signals were observed for 1h, 2h, 3h and 6h, respectively. The total number of seeded cells in the co-culture condition varied (low : 1×10^5 , mid: 5×10^5 , high: 1×10^6 perwell) Nucleus (Blue), F-actin (Green), PpIX (Red). Scale bar, 100 μm .



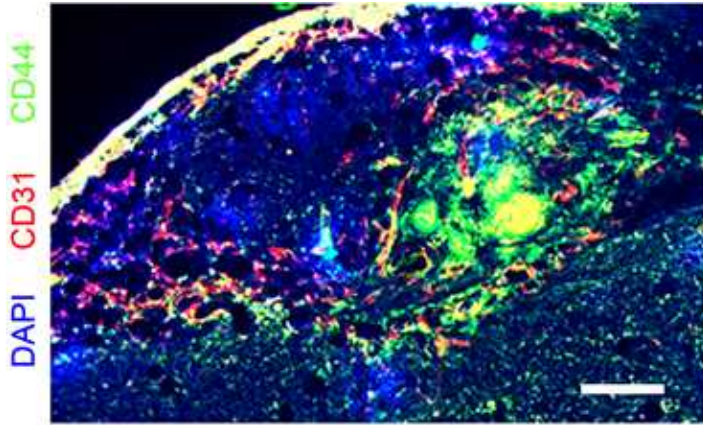
Supplementary Figure 8. Fluorescence images of selective turn on fluorescence signals generated by nanocarriers in a co-culture condition with the mixture of MKN-45 cells and human fibroblast cells. The fluorescence signals were observed for 1h, 2h, 3h and 6h, respectively. The total number of seeded cells in the co-culture condition varied (low : 1×10^5 , mid: 5×10^5 , high: 1×10^6 perwell) Nucleus (Blue), F-actin (Green), PpIX (Red). Scale bar, 100 μm .



Supplementary Figure 9. Fluorescence images of selective turn on fluorescence signals generated by nanocarriers in a co-culture condition with the mixture of C6 cells and MKN-74 cells. The fluorescence signals were observed for 1h, 2h, 3h and 6h, respectively. The total number of seeded cells in the co-culture condition varied (low : 1×10^5 , mid: 5×10^5 , high: 1×10^6 per well) Nucleus (Blue), F-actin (Green), PpIX (Red). Scale bar, 100 μm .



Supplementary Figure 10. IVIS Images of mice. All mice were conducted by repeated injection of nanocarrier and time-dependent imaging in day 3 and day 14 respectively. The mice (Group 1, n=5) administrated nanocarriers, and the mice (Group 2, n=3) as a control group administrated free 5-ALA.



Supplementary Figure 11. Fluorescence immuno-labeling analysis. A representative microscopy image of sectioned tumors, illustrating localization of Nuclei (DAPI; blue), CD44 (green), CD31 (blue).

Publication List

- (1) Jeong, Y.; Kim, G.; Lee, B.; Kim, S.; Koh, W.; and Lee, K. "Lighthouse for cancer: Selective navigation of fluorescence turn on nanocarrier " not published yet

암 표적형 형광전구체를 담지하고 있는 생체친화성 나노전달체의 제조

정 윤

나노융합과

융합과학부

서울대학교 융합과학기술대학원

나노입자 기반 형광 진단기술은 체내에서 형광민감도가 급격히 떨어지거나, 인체 내 안전성 문제에서 자유롭지 못하다. 또한, 지금까지 개발된 대부분의 기술들이 여러 단계를 거치는 복잡한 제조 공정으로 인해 상용화를 위한 근본적인 연구 방향과는 거리가 멀어진다. 그 중에서도 생체 안정성이 검증된 소수 후보군의 나노물질만이 의약품 임상시험계획 승인을 받은 후, 임상 연구단계로 진입할 수 있다. 결국, 위와 같은 나노기술을 활용한 형광 진단 연구가 가지고 있는 한계점을 극복하기 위하여 새로운 기술이 적극 필요한 상황이다.

본 연구에서는, 기존 나노입자 기반 형광 질병진단 및 응용기술이 가지고 있는 근본적인 문제점을 해결하고자, 새로운 형태의 천연고분자 기반 암세포 표적형 형광신호 발광이 가능한 나노전달체를 제조하였다. 나노전달체는 체내 존재하는 천연 고분자인 히알루론산을 주골격으로 하고 있다. 동시에, 히알루론산은 암세포 표면에 과발현되는 당단백의 한 종류

인 CD44에 선택적 반응하기 때문에 나노전달체 자체에 암세포 표적성을 부여한다. 암세포의 선택적 형광 신호 발광을 위하여 형광전구체 물질인 5-아미노레블린산을 나노전달체 내부에 비공유 결합으로 담지하였다. 5-아미노레블린산은 세포 내로 유입된 후 생합성 과정을 통해 형광 물질인 프로토포르피린 IX로 전환된 후 체내에서 분해된다. 천연물로만 구성된 나노전달체의 제조 및 형광 전구체의 생합성 발광 메커니즘을 활용한 암세포 및 동물모델 연구 결과를 본문에 제시하였다.